Biosensors and Bioelectronics 82 (2016) 64–70

Contents lists available at ScienceDirect

Biosensors and Bioelectronics

journal homepage: www.elsevier.com/locate/bios

Early detection of skin cancer via terahertz spectral profiling and 3D imaging

Anis Rahman [a,*], Aunik K. Rahman [a], Babar Rao [b]

[a] Applied Research & Photonics, 470 Friendship Road, Suite 10, Harrisburg, PA 17111, United States
[b] Rutgers University, 1 Worlds Fair Drive, Suite 2400, Somerset, NJ 08873, United States

ARTICLE INFO

Article history:
Received 25 July 2015
Received in revised form
19 January 2016
Accepted 21 March 2016
Available online 22 March 2016

Keywords:
Terahertz scanning reflectometry
Skin cancer
Early detection
Basal cell carcinoma
Terahertz time-domain spectrometry
Terahertz 3D imaging
Terahertz skin layer profiling

ABSTRACT

Terahertz scanning reflectometry, terahertz 3D imaging and terahertz time-domain spectroscopy have been used to identify features in human skin biopsy samples diagnosed for basal cell carcinoma (BCC) and compared with healthy skin samples. It was found from the 3D images that the healthy skin samples exhibit regular cellular pattern while the BCC skin samples indicate lack of regular cell pattern. The skin is a highly layered structure organ; this is evident from the thickness profile via a scan through the thickness of the healthy skin samples, where, the reflected intensity of the terahertz beam exhibits fluctuations originating from different skin layers. Compared to the healthy skin samples, the BCC samples' profiles exhibit significantly diminished layer definition; thus indicating a lack of cellular order. In addition, terahertz time-domain spectroscopy reveals significant and quantifiable differences between the healthy and BCC skin samples. Thus, a combination of three different terahertz techniques constitutes a conclusive route for detecting the BCC condition on a cellular level compared to the healthy skin.

1. Introduction

Terahertz scanning reflectometry offers an opportunity to investigate both the surface and the sub-surface of biological tissues (e.g., skin) by non-invasive means. The non-ionizing nature of terahertz radiation (T-ray) eliminates radiation damage or perturbation of sensitive tissues while still able to probe disease conditions in the deeper layers leading to an effective early diagnostic tool. For example, thickness profiling of healthy and cancerous skin tissues would show vast differences in their profiles. In this study, terahertz techniques have been developed that are comprised of terahertz scanning reflectometry, terahertz time-domain spectroscopy and terahertz 3D imaging (all instruments from Applied Research & Photonics, Harrisburg, PA 17111) for detection of cancerous skin with basal cell carcinoma (BCC) in comparison with healthy skin samples. Two groups of samples were investigated; the first group of samples is healthy skin biopsy and the second group of samples is biopsy from cancerous area. Thickness profiling exhibits significant differences in profiles of the respective skin samples both in their layer structure and also in their total reflected intensities; thus, indicating presence and lack of cellular order for the respective specimens. Similarly, terahertz spectra acquired in transmission exhibit quantifiable differences for both groups of samples. More interestingly, 3D terahertz image of the healthy skin shows regular cell patterns while the image of samples with BCC exhibits no clear cell pattern. The lack of clear cellular order in the skin, thus, may be used as an indication of cancerous area and this finding may be used as an early diagnostic tool.

Skin biopsy remains the gold standard in skin cancer diagnosis; however non-invasive and more cost effective diagnostic tools may be a reasonable alternative for clinicians and patients. Reflectance confocal microscopy is a non-invasive imaging technique that allows visualization of the skin at the cellular level with higher sensitivity and specificity. However, its wide scale use is limited due to the cost of equipment and image interpretation is complicated. Confocal imaging suffers from the disadvantages that the signal strength is reduced by requirement for detector pinhole, thus, restricting the image field. The pinhole also reduces the signal to noise ratio and thus, increases noise sensitivity. Additionally, the technique is more labor intensive and requires more training and experience to be successful ("Confocal Imaging" by Kroto Imaging Facility (2016); Rajadhyaksha et al. (1999); Calzavara-Pinton et al. (2008)).

Spectrophotometric intracutaneous analysis is another multispectral imaging (MSI) technology that depends on chromophores mapping to determine microscopic architecture. Its accuracy is better in assessing the amount of melanin and collagen present in the skin, but the histologic correlation is weak (Matts and Cotton, 2010). MelaFind, another MSI system, uses pattern-recognition

* Corresponding author.
E-mail address: a.rahman@arphotonics.net (A. Rahman).

http://dx.doi.org/10.1016/j.bios.2016.03.051
0956-5663/

algorithms to study clinically atypical pigmented skin, thus, augments biopsy sensitivity but decreases specificity (Gutkowicz-Krusin et al., 2000). Electrical impedance spectroscopy (EIS) studies resistance to the flow of alternating current through tissues and correlates it to underlying structural changes (Morimoto et al., 1993). EIS devices have low specificity, are expensive and require complex data analysis for quantification. Optical coherence tomography (OCT) uses infrared light to study skin up to a depth of ~2 mm. On its own, the device has low specificity but it can be combined with dermoscopy, high- frequency ultrasound or confocal reflectance microscopy to complement noninvasive diagnosis. OCT also requires additional contrast enhancement. A noted difficulty with OCT is that the system cannot image well the aortic ostial lesions. There is no way to clear the blood from the aorta at the entrance to right or left main arteries, so it is difficult to get clear images of these areas (Fornell, 2011). Another principal disadvantage of OCT imaging is that light is highly scattered by most biologic tissues. It is reported to be the best for optically transparent tissues. Skin being non-transparent, therefore, is not best studied by OCT (Qaum, 2000).

From the above considerations, use of terahertz technology offers the promise of overcoming the above mentioned deficiencies by implementing a self-cross-checking technique. In what follows, we describe the terahertz methods utilized for the current investigations followed by the results, discussion and conclusions.

2. Materials and methods

2.1. Thickness profile determination

Fig. 1 exhibits the concept of a continuous wave terahertz scanning reflectometer (CWTSR) measurement system; the principle of measurement was reported elsewhere (Rahman et al., 2012). Briefly, a CW terahertz source is used that generates the terahertz radiation from an electro-optic dendrimer via dendrimer dipole excitation (Rahman and Rahman, 2012). As shown in Fig. 1, the terahertz beam is focused on the specimen at 90° angle via an off-axis parabolic reflector (normal incidence). The beam reflected by the substrate is directed to the detection system via a beam splitter/combiner. The specimen cell is comprised of a scanning

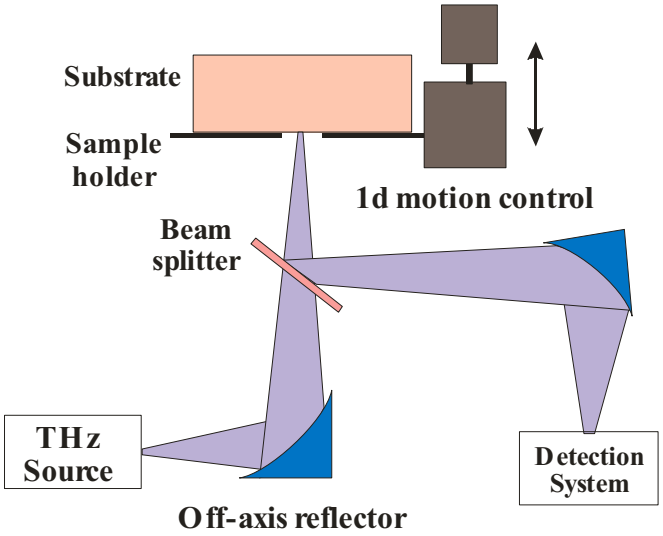

Fig. 1. Experimental setup of the terahertz scanning reflectometer. A fine pitch motion control system is used to move the substrate (sample holder) in and out of the focal point while the detection system may acquire data in real-time. For kinetics, the specimen is kept fixed and focused.

platform that is controlled by a high precision motion control system. This arrangement allows direct measurements as follows. The off-axis parabolic reflector is adjusted such that initially the terahertz beam remains focused on the substrate surface. At this position the Z-axis of the motion control can be engaged for scanning the substrate to interrogate the reflectance across its thickness.

Under the assumption that the reflectance is proportional to the physical properties of the incident layer (e.g., the refractive index or density), a vertical scan will produce the thickness profile of the substrate, as explained below.

The motion control can be engaged to move the focal point inside the substrate to interrogate the reflectance at the point of incidence and then gradually across the thickness; this gives an array of $\partial R/\partial x$ corresponding to the point of incidence, where R is the reflected intensity. Assuming R is a function of the physical properties of the substrate, the gradient of a specific property is measured directly by measuring R. A similar scan is also done for the empty holder. The reflectance of the blank holder (reference) is subtracted from the reflectance of the specimen to compute the profile:

$$\left|\frac{\partial R}{\partial x}\right|_{Specimen} = \left|\left|\frac{\partial R}{\partial x}\right|_{SampleScan} - \left|\frac{\partial R}{\partial x}\right|_{Reference}\right| \quad (1)$$

The measured reflectance, thus, may be utilized to deduce the layer-structure of the specimen by point-by-point scanning across the whole thickness. The current scanner has a resolution of ~25 nm. Since the human skin cells are a few microns in diameter, a scanning resolution of a few tens of nanometer is sufficient for the profile generation.

Further, the Z-axis may be locked on a given layer and an area scan may be conducted to generate a surface plot of that layer. When a XYZ scan is conducted, a 3D reconstructed image may be generated by sequential layer by layer scan. More on the reconstructive imaging is discussed later.

2.2. Terahertz time-domain spectroscopy

When THz radiation interacts with the skin cell molecules, it will stimulate many resonances such as molecular vibrations, and/or other resonances due to translation, rotation, torsion, and even conformational changes of the molecules. Therefore, terahertz interaction will result in the incident photons being affected by characteristic quantities determined by a specific interaction (Rahman, 2011) or by multiple interactions. The change in energy and/or frequency yields information about the molecular nature of the interaction. Molecular simulation, especially molecular dynamics, reveals that there are numerous resonances and conformational states possible when a molecule is not at its lowest energy state (Rahman, et al., 1999). As most materials remain at their lowest energy state under normal and steady state conditions, terahertz perturbation will stimulate possible available transitions. Therefore, the transmitted beam will carry information about the matrix; and equivalently the reflected beam will also carry information about the nature of the material. Quantitative prediction of such information is obviously materials specific and best determined by experimental measurements. Notably, biological systems are almost never at equilibrium. Hence, terahertz interactions may also be exploited to study the dynamic nature of a biological system.

2.3. Reconstructive imaging

The intensity of the reflected terahertz beam is proportional to the specific features of the specimen under test. Therefore,

measured intensity may be modeled in terms of suitable physical parameters such as refractive index, density, dielectric function, etc., via a modified Beer-Lambert's law. If all material parameters are assumed to remain unchanged during measurement, because, terahertz radiation is non-ionizing and does not perturb the intrinsic properties, then the reflectance, R, will be proportional to the variations in material properties at the point where the beam is incident. For human skin, although a wide variation of physical properties such as density is not expected, however, water and fat contents of different layers of skin will vary. As such, the reflectance is dependent on the spatial and angular coordinates: $R(x, y, z, \theta)$. Therefore, a 3D reconstructed image generated from reflectance will yield the characteristic cellular patterns of the skin. Another advantage of the terahertz scanner is that the scanning is conducted across the thickness of skin for interrogation of internal layers in a non-contact mode. This is only possible with terahertz radiation because the energy is capable of penetrating inside the skin without any harmful effect. Based on the above principle, a signature of a given feature may be established. Moreover, feature size may be estimated from either a 2-D scanned or 3-D scanned reconstructed imaging. The terahertz nano-scanner deploys a non-contact measurement system with an adjustable stand-off distance. The sample space is adjustable to accommodate required sample size. A rotary axis enables examination of a sample from different viewing angles. This is important because some features and non-uniformities might not be along a straight line-of-sight. Thus an angular scan enables viewing hidden features. In addition, with the advent of the angular axis, one can scan cylindrical objects in a conformal fashion.

2.4. Experimental

Fig. 2 shows a cartoon of different anatomical features of human skin cross section. A vertical scan (thickness profile) is thus expected to exhibit layering information. However, it can also be assumed from Fig. 2 that the layering pattern will be different at different spots on the skin because the thickness profile is not the same at every place. It is expected that a layered pattern of some kind will be present for the healthy skin while the cancerous skin will exhibit diminished layered structure due either to cell agglomeration or other deformation; and thus, loss of regular cellular pattern that eventually may form a tumor. Other lesions are also expected to exhibit their characteristic pattern, thus being detectable by this technique.

For the present study, excised skin tissue samples were collected from consenting patients undergoing Mohs' Micrographic Surgery. These skin samples were stored in dry ice until a few minutes before the measurements. Thickness profiles, terahertz spectra, and reconstructed image scans were taken within two days of collecting the samples. Samples were taken from four different patients. Some of these samples were benign, non-cancerous and some were diagnosed for basal cell carcinoma.

All samples were mounted one by one on a high density polyethylene (HDPE) holder. Measurements were done one at a time, thus the same background was valid for all measurements. For example, a healthy sample (14–50a) was attached on the HDPE holder and loaded into the CWTSR, and thickness profile was recorded. This sample on the same holder was then loaded into the terahertz time-domain spectrometer, TeraSpectra. Terahertz spectrum was recoded with the spectrometer's front-end software. Thickness profiles and terahertz spectra were taken in the same manner for each remaining samples. Additionally, a few samples were mounted on a nano-scanner for ZYX scanning for reconstructive imaging. Thickness profiles, terahertz spectra, and reconstructed images were analyzed to study the characteristic features of the healthy and cancerous skin tissues and to assess any significant differences between them.

3. Results

3.1. Thickness profile

Fig. 3 exhibits thickness profile of the empty cell; this is used as the reference for all subsequent measurements. Several trials were taken at an interval of ~5 min that were averaged to obtain the average reference; Ref_{Av}. Average error limit was calculated to be ± 2295 counts. Since the maximum reflection value of the healthy skin sample is 8.785×10^6, this corresponds to a signal to noise ratio of $\sim 3.8 \times 10^3$. Fig. 4 shows the thickness profile scan of a healthy skin sample (14-51A, left Y-axis). The skin thickness profile (right Y-axis) is obtained by subtracting the reference (Fig. 3) from the scan of the skin sample. As seen from Fig. 4 (right Y-axis), the reflected intensity exhibits increasing trend as the beam's focal point is penetrated through the skin thickness up to ~530 μm. The fluctuations in the intensity are indicative of the layered structure of the skin. As the beam penetrates deeper, more photons are

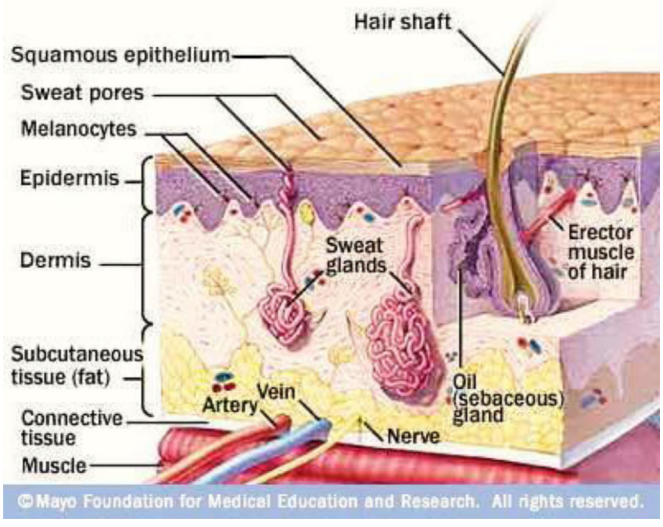

Fig. 2. Anatomy of the human skin showing different constituents and layers (adapted).

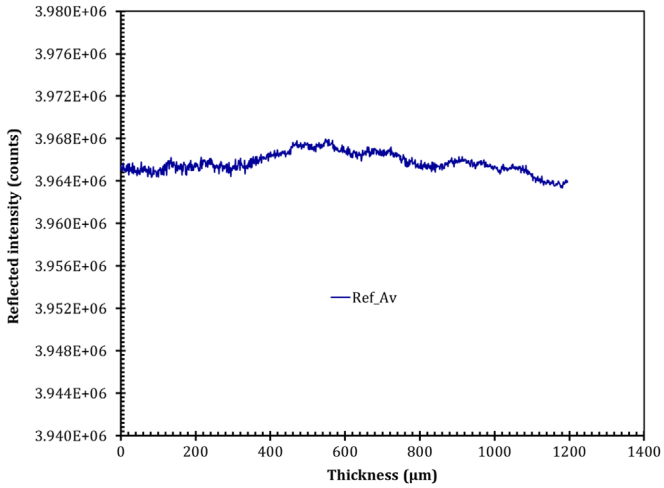

Fig. 3. Thickness profile of empty cell used as the reference. Several trials were taken at an interval of 5 min. Trials were averaged to obtain the Ref_{Av}. Average error limit was calculated to be ± 2295 counts.

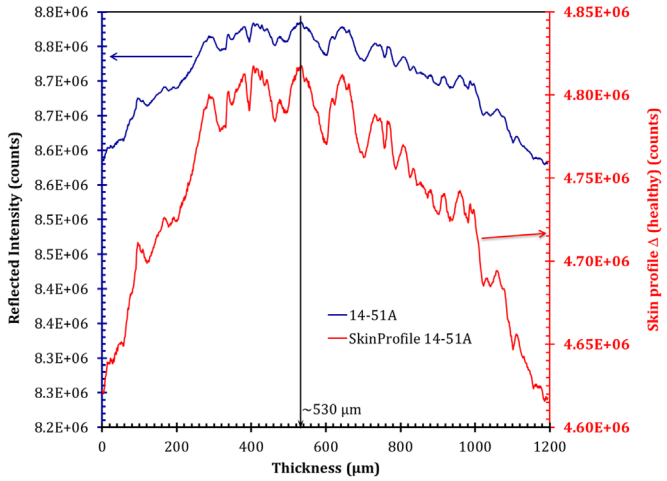

Fig. 4. Thickness profile from scan of a healthy skin sample (14-51A, left Y-axis). The skin thickness profile (right Y-axis) is obtained by subtracting the reference from Fig. 3. The reflected intensity increases as the beam focal point is penetrated through the skin thickness indicating layering of the skin. As the beam penetrates deeper, more photons are absorbed by the skin cells of different layers. Also some energy is escaped via transmission, thus decreasing the reflected intensity.

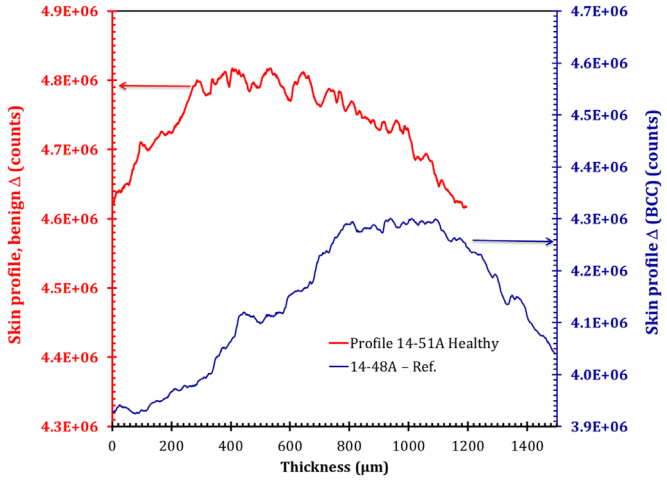

Fig. 5. Thickness profile of healthy skin (left Y-axis, red curve) and skin with basal cell carcinoma (right Y-axis, blue curve). The BCC skin sample (14-48A) has a lower reflectance compared to the healthy sample. (For interpretation of the references to color in this figure legend, the reader is referred to the web version of this article.)

absorbed by the skin cells of different layers and some are escaped via transmission through the skin; thus, decreasing the reflected intensity beyond 530 μm up to ~1.2 mm. A clear layering pattern is also visible from this plot. Fig. 5 shows the thickness profiles of healthy skin (left Y-axis) and a sample with basal cell carcinoma (right Y-axis). These profiles exhibit significant differences between the healthy and cancerous skin profiles both in their layer structure and also in their total reflected intensities. The presence of layers is visible for the healthy skin while the layer definition of BCC sample is clearly diminished. Also, the cancerous skin exhibits lower reflected intensity (right Y-axis of Fig. 5) compared to healthy skin sample (Fig. 5, left Y-axis). This is indicative of a higher reflectivity of healthy skin due its regular cellular order while the lack of regular cell pattern of the BCC sample is indicative of either absorbing more T-ray or being relatively more transparent or both. However, scattering may also play a role for lowering the reflected intensity by the BCC samples. But since the healthy skin has a regular cellular order and the BCC skin samples have a diminished cellular order, it is likely that the healthy skin will scatter more than the BCC skin. If this was the case, then healthy skin was expected to exhibit a lower reflected intensity. The present observations are contrary to this hypothesis. As such it is assumed that the most likely cause of lower reflected intensity from the BCC samples is due to absorption and/or escaped energy through the diminished cellular order of these samples.

3.2. Time-domain spectroscopy

Terahertz time domain spectroscopy was conducted on both groups of samples. Fig. 6 shows a skin sample mounted on a HDPE holder (left). The HDPE holder has an opening for terahertz transmission through the specimen without being barred by the HDPE. The specimen is mounted on the spectrometer and placed in the beam path with the help of a XYZ positioning stage (Fig. 6, right). An iris is used to limit the beam such that the central part of the specimen is exposed; this ensures all specimens are exposed in the same way with identical input intensity. The time-domain signal is acquired by the front-end software of the spectrometer. Fig. 7 shows the time-domain signal (interferogram) of a healthy skin sample (left) and a BCC biopsy sample (right). Both samples were mounted on the same holder, one at a time and spectra were acquired successively. Thus it was ensured that both samples have identical background. As seen from Fig. 7, the time-domain signal of the sample with BCC is significantly different than that of the healthy skin sample. It is noted that the transmitted intensity of the BCC skin sample is higher than that of the healthy skin sample. This is consistent with the findings from thickness profile (Fig. 5) where the BCC skin sample has a lower reflectance than the healthy skin sample. Fourier transform is conducted as a standard practice for extracting frequency domain spectra from the time-domain signal (interferogram). However, because of very high sensitivity of terahertz interaction with materials, usually the Fourier transform will result in to a multitude of peaks in the frequency spectrum (Rahman, 2011). Often there is no ready explanation of many of these peaks in the absorbance spectrum, for example, for nonstandard soft material such as human skin. Hence it is advantageous to reduce the number of peaks to a few characteristics ones. Therefore, we conducted a different procedure, the Eigen Frequency analysis (Marple, 1987). Eigenvalues and eigenvectors are properties of a mathematical matrix. When the matrix is composed of a given material parameters, then one can extract particular property of interest. Eigen analysis frequency estimation algorithms offer high-resolution frequency estimation. These procedures are perhaps the most accurate procedures for estimating harmonic frequencies.

Fig. 8 exhibits the Eigen frequency absorbance spectra corresponding to the time-domain signal or interferogram shown in Fig. 7. Here the healthy and BCC skin samples yield their respective spectral signatures. It is observed that the BCC samples have a higher absorbance (or equivalently, lower reflectance) compared to that of the healthy samples. This is consistent with the observation for the thickness profiles where a less structured layering was observed for the BCC samples with lower reflectance while the healthy samples showed pronounced layered structure with higher reflectance.

3.3. Reconstructed imaging

Fig. 9 shows the reconstructed 3D image of a healthy skin sample (left) and a skin sample with basal cell carcinoma (right). Healthy sample was scanned over 1 mm × 1 mm × 1.2 mm and the BCC sample was scanned over 1 mm × 1 mm × 1.4 mm, because, the cancerous skin is thicker than the healthy skin. The top surface of healthy skin shows regular cell pattern (left) while the BCC sample exhibits a lack of regular cell patterns. This regular cell pattern of the healthy skin sample is also visible throughout its

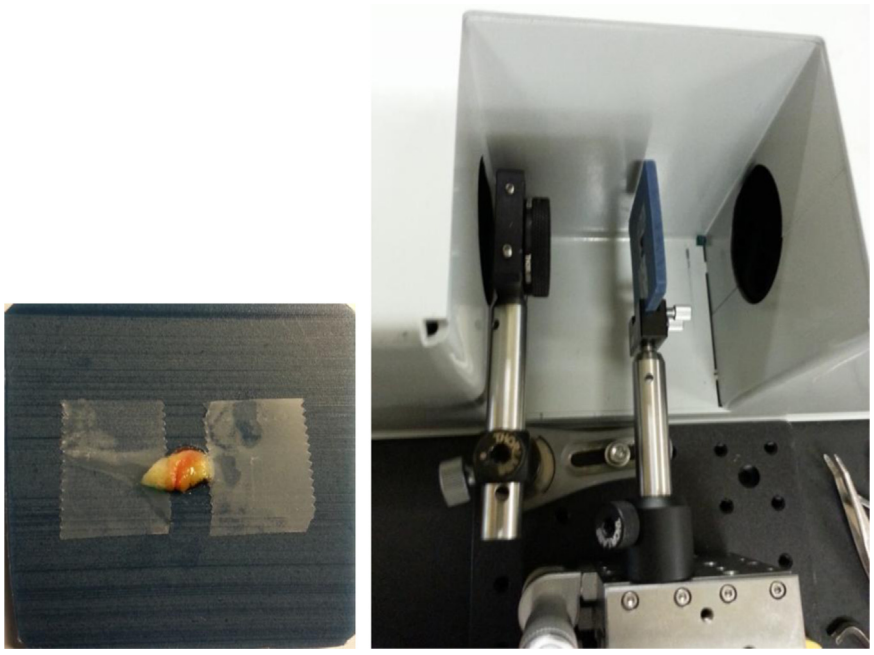

Fig. 6. A biopsy skin sample is fixed on a high density polyethylene plate (left) used as the sample cell that has an opening for terahertz transmission only through the specimen. The cell is then mounted on the spectrometer (right) and the specimen is placed in the beam path with the help of a XYZ positioning stage. An iris is used to limit the beam such that the central part of the specimen is exposed.

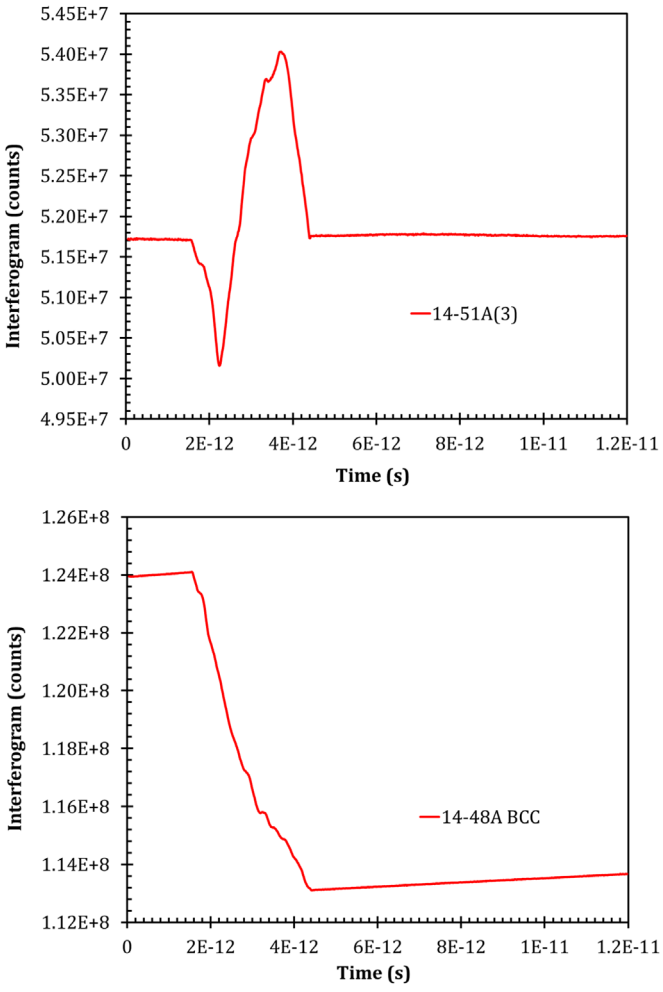

Fig. 7. Time-domain signal (interferogram) of healthy skin sample (above) and BCC biopsy sample (below).

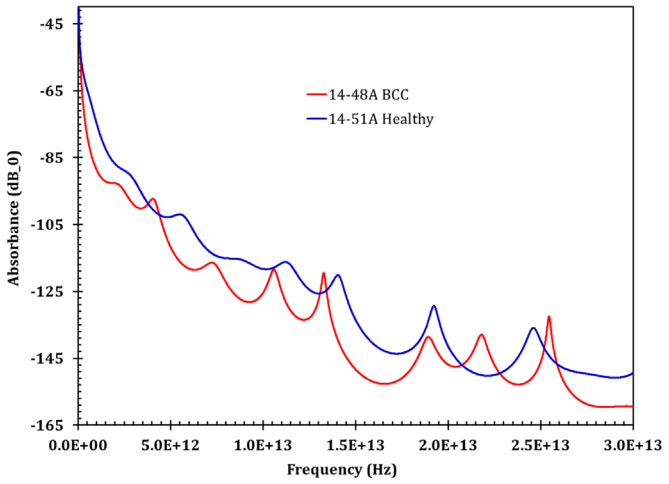

Fig. 8. Eigen frequency absorbance spectra of healthy and cancerous skin samples. Healthy skin shows lower absorbance compared to the BCC skin. However, some of the peaks of the healthy skin sample are not present in the BCC sample. The thickness of the measured healthy skin samples is ~1.2 mm and that of the BCC samples is ~1.4 mm.

thickness. Therefore, the lack of normal cellular pattern is indicative of cell agglomeration due to BCC. This feature, thus, may be used as a metric for early detection of the BCC. Fig. 10 shows the images of a stack of a number of slices of the healthy skin sample at arbitrary intervals across the thickness and Fig. 11 shows the same for the sample with BCC. These Figs. demonstrate the ability that once the 3D measurements are done, the skin profile may be examined on a layer by layer basis. The thickness of every slice may also be tuned either by adjusting the scan interval or by post scan data analysis via built-in gridding algorithm.

4. Discussion

In light of the foregoing results, it is clear that the techniques reported in this paper have a strong potential for effective

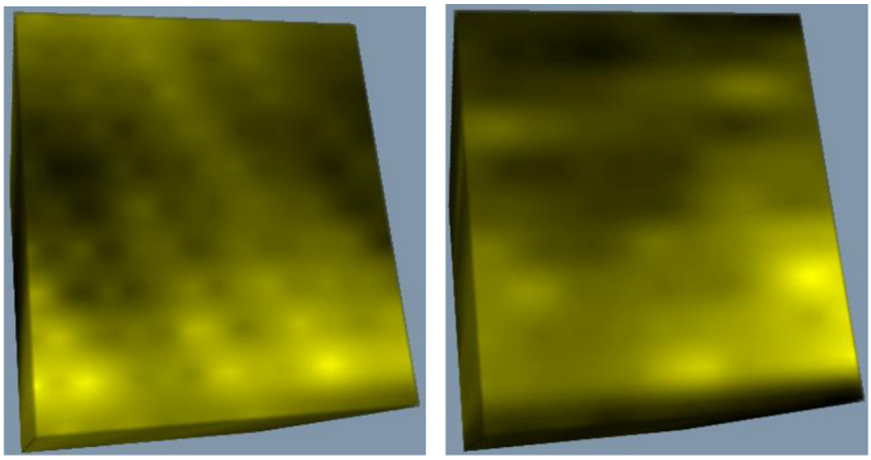

Fig. 9. Reconstructed 3D image of healthy skin (left) and skin with basal cell carcinoma. Healthy sample was scanned over 1 mm × 1 mm × 1.2 mm and BCC sample was scanned over 1 mm × 1 mm × 1.4 mm. The top surface of healthy skin shows regular cell pattern (left) while the BCC samples has lost regular cell patterns and exhibit more agglomerated structure. This is also seen throughout the thickness of the sample.

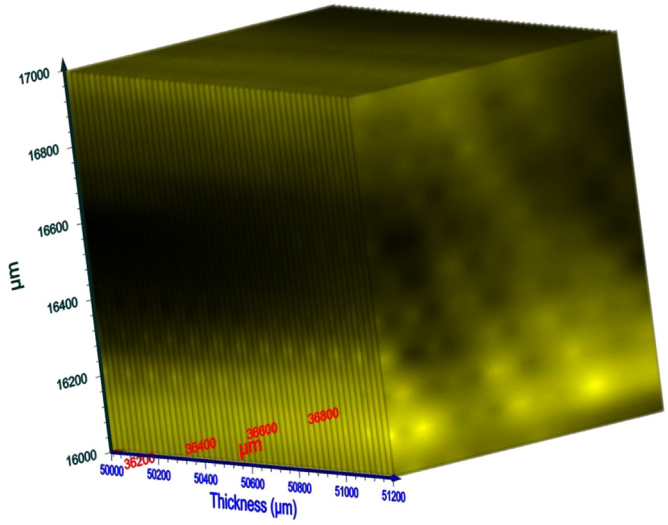

Fig. 10. Slices of the 3D image across the thickness of a healthy skin sample; thickness is ~1.2 mm, represented along the vertical axis (Z-axis, blue). This indicates the layer by layer inspection capability. (For interpretation of the references to color in this figure legend, the reader is referred to the web version of this article.)

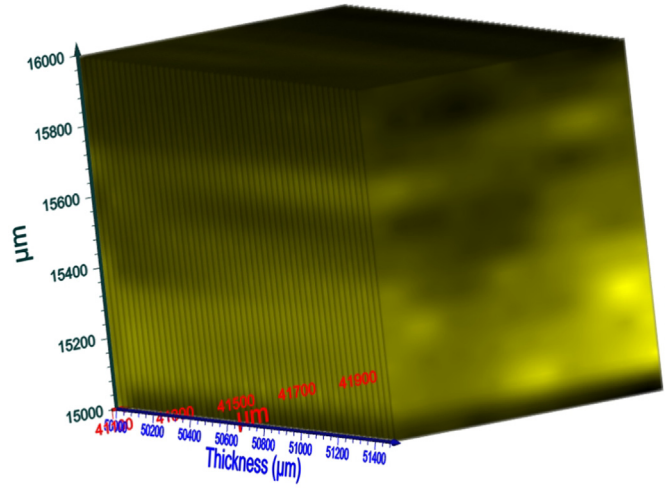

Fig. 11. Slices of the 3D image across the thickness of a BCC skin sample; thickness is ~1.4 mm. This indicates the layer by layer inspection capability.

diagnosis of early stage skin cancer. However, there are other considerations that need to be addressed before a final diagnostic tool may be presented to the dermal and transdermal community. In particular, methodology should be developed to identify healthy tumor vs malignant ones; basal cell carcinoma vs a seborrheic Keratosis, which is benign; or a healthy mole vs early melanoma. As indicated by the present results, each of the three techniques is capable of discerning healthy versus diseased samples in their own right. Once the signature by individual techniques are established for each of the skin conditions, then a suitable algorithm should be able to utilize the data from each technique to arrive at a conclusive diagnosis. The next investigations will be geared toward this goal.

5. Conclusions

Terahertz technology has been deployed for detection of skin cancer, viz., the basal cell carcinoma. Three different terahertz techniques have been exploited including scanning reflectometry for thickness profiling, time-domain spectrometry for spectral analysis and high resolution 3D reconstructed imaging for visual inspection of cancerous versus healthy skin samples. Combination of the three techniques is expected to produce a fool-proof diagnostic tool. Both healthy (benign) skin biopsy samples and the biopsy from cancerous area were investigated. Respective thickness profiles exhibit a highly layered structure for healthy skin samples while the layering structure is diminished for the BCC skin. Also the total reflected intensity for the healthy skin is higher than the BCC skin; thus indicating presence and lack of cellular order for the respective specimens. Transmission mode Terahertz spectra exhibit quantifiable differences for both kinds of samples. Finally, 3D terahertz image of the benign skin shows regular cell patterns while the images of BCC sample exhibit irregular and/or agglomerated cell patterns. The lack of cellular order in the skin, thus, may be used as an indication of cancer forming process with the exclusion of the conditions discussed in Section 4. These results, therefore, may be utilized for creating an early diagnostic tool. It is notable that this is the first of such a concerted observation of healthy versus BCC skin samples with three different experiments. The results are consistent from individual experiments and collectively provide an accurate means of early detection of BCC.

References

Calzavara-Pinton, P., Longo, C., Venturini, M., Sala, R., Pellacani, G., 2008. Photochem. Photobiol. 84 (6), 1421–1430.

Fornell, D., 2011. The Advantages and Disadvantages of OCT vs. IVUS, Feature, May 18, ⟨http://www.dicardiology.com/article/advantages-and-disadvantages-oct-vs-ivus⟩.

Gutkowicz-Krusin, D., Elbaum, M., Jacobs, A., 2000. Melanoma Res. 10 (6), 563–570.

Kroto Imaging Facility, 2016. Confocal Imaging. ⟨https://www.sheffield.ac.uk/kroto/confocal/confocal_imaging⟩.

Marple Jr., S.L., 1987. Digital Spectral Analysis with Applications. Prentice Hall, Upper Saddle River, pp. 361–378.

Matts, P.J., Cotton, S.D., 2010. Handbook of Cosmetic Science and Technology, 3rd ed. CRC Press, Boca Raton, pp. 275–281.

Morimoto, T., Kimura, S., Konishi, Y., et al., 1993. J. Invest. Surg. 6 (1), 25–32.

Qaum, T., 2000. Optical Coherence Tomography & Ultrasound Biomicroscopy of the Eye, September, ⟨http://eradiology.bidmc.harvard.edu/LearningLab/central/qaum.pdf⟩.

Rahman, A., Durning, C.J., Turro, N.J., 1999. Molecular Dynamics of PAMAM Dendrimers (unpublished) ⟨http://arphotonics.net/PAMAM%20Dynamics%20report1up.pdf⟩.

Rahman, A., 2011. J. Mol. Struct. 1006, 59–65.

Rahman, A., Frenchek, S., Brian, K., Patterkine, L., Rahman, A., Michniak-Kohn, B., 2012. Drug. Dev. Deliv. 12 (4), 43–49.

Rahman. A., Rahman, A., 2012. Wide range broadband terahertz emission from gigh $\chi(2)$ dendrimer, in: Sadwick, L.P, O'Sullivan, C.M., (Eds.) Terahertz Technology and Applications V, Proc. SPIE, 8261, 82610H-1–82610H-6.

Rajadhyaksha, M., Gonzalez, S., Zavislan, J.M., Anderson, R.R., Webb, R.H., 1999. J. Invest. Dermatol. 113 (3), 293–303.